12th International Congress on the Deterioration and Conservation of Stone
Columbia University, New York, 2012

MONITORING FROST SUSCEPTIBILITY OF LIMESTONE FACIES

Tim De Kock,[1,a] Marijn Boone,[1] Jan Dewanckele,[1] Wesley De Boever,[1] Delphine Vandevoorde,[1,5] Matthieu Boone,[2] Geert De Schutter,[3] Eberhard Lehmann,[5] Patric Jacobs[1] and Veerle Cnudde[1]

[1] *UGCT- Research Group Sedimentary Geology and Engineering Geology, Department of Geology and Soil Science, Faculty of Sciences, Ghent University, Belgium.*
[2] *UGCT- Radiation Physics Research Group, Department of Physics and Astronomy, Faculty of Sciences, Ghent University, Belgium*
[3] *Magnel Laboratory for Concrete Research, Department of Structural Engineering, Faculty of Engineering, Ghent University, Belgium.*
[4] *Department of Conservation and Restoration, Artesis University College of Antwerp, Mutsaardstraat 31, 2000 Antwerp, Belgium*
[5] *Neutron Imaging and Activation Group, PSI, CH-5232 Villigen, Switzerland*

Abstract

Limestones are among the most frequently used building stones worldwide. Their frost susceptibility has been assessed in many ways, but due to the large amount of existing limestone types and the natural stone heterogeneity, laboratory testing of the freeze-thaw resistance remains a necessary testing method to predict their behavior when used as a building stone. In this research, the frost susceptibility of some frequently used French building stones from the Oolithe Blanche Formation is assessed indirectly and directly in several ways by laboratory testing. The selected stones have similar components (ooids and bioclasts) but differ in dolomite content and thus porosity distribution, resulting in dissimilar water transport properties. The results of experimental freeze-thaw cycles are coupled to the water absorption by capillarity and the saturation coefficient through water imbibition. Mechanical properties as flexural strength provide additional information. Experiments with neutron radiography and X-ray microtomography allow to visualize the water absorption pathways inside the stones. X-ray allows to visualize and quantify the changes in pore structure and the damage propagation.

Keywords: freeze-thaw, Massangis, microstructure, dolomitization, X-ray µCT

1. Introduction

Limestone from the Oolithe Blanche Formation (Bathonian) are quarried in several places in the Yonne Department (France) to use as building and dimension stones. In this region the Formation is approximately 80 meters thick and well-studied, e.g. for CO_2 storage (Casteleyn *et al.*, 2010). The excavated material is mostly marketed under the name of the location where they are quarried, which is illustrated by names such as Anstrude, Massangis and Vaurion. The Bathonian deposits belong to the Mesozoic sediments of the Paris Basin. Several active and abandoned quarries exist in the neighborhood of the town Massangis, exploited by different owners and with recent activities dating back to 1889 (Dessandier, 2006). Stones from this region play a big role

on the Belgian market. They are used in several outdoor applications both in new buildings as well as for renovation purposes. They are frequently used as replacement material for the local historic building stone called the 'Lede stone' or 'Balegem stone' (Camerman, 1957). Their use became so obvious for restoration purposes of this Lede stone in Belgium, it was called 'massangitis' (Breda, 2005). Nevertheless, Lede stone is a greyish-greenish arenaceous limestone with ochre patina whereas the Massangis is a grey-yellow pure limestone with a pale patina. As such, both esthetical effects after patina formation as well as the microstructure of both stones varies tremendously.

A natural variability exists within the Massangis quarries. Distinctions are mainly based on color, with variants named 'Massangis Claire' and 'Massangis Jaune'. In between, varieties such as 'Massangis Jaune Claire' exist as well. These variants are not regular bedded within the quarry, but rather occur as irregular zones crosscutting the bedding. Studies attributed to this building material report dolomitization/dedolomitization processes as a cause for this variability (Elsen *et al.*, 2005). Since it is stated that they show a difference in freeze-thaw resistance, it is advised to prefer the Massangis Jaune for outdoor applications, as the Massangis Claire is more prone to freeze-thaw deterioration.

Freeze-thaw deterioration is a major cause of damage to natural building stones in moderate and humid climates (Ruedrich and Siegesmund, 2007). The plausible processes causing freeze-thaw deterioration are thoroughly discussed in literature. Two main processes are considered to be volumetric expansion and ice segregation. The first theory is based on the volumetric expansion of approximately 9 % when water freezes to ice at 0° C to 13.5 % at -22° C (Tharp, 1987), exerting pressure on the rock. This damage process requires a high water saturation and rapid freezing and will be limited to the upper few exposed centimeters in diurnal frost cycles (Matsuoka & Murton, 2008). In fact, in 1908, Hirschwald based his saturation coefficient on this volumetric expansion as a first assessment on a rock's frost resistance (Camerman, 1957). In addition, hydrofracture can be related to this process when the volumetric expansion expels pore water and therefore creates a hydraulic pressure.

The ice segregation theory was parallelized from the frost heaving of soils by Walder & Hallet in 1985 and 1986. Based on thermodynamics, they argued the formation of ice lenses due to suction of pore-waters in capillaries and adsorbed on mineral surfaces towards a freezing site to continue the growth of an ice lens, thus exerting a pressure by its growth. They state that repeated low-amplitude cycling at 0 °C may never bring the rock into the favored regime, whereas temperatures in the range of roughly -5 °C to -15° C may favor crack growth. Empirical and physical and numerical modeling (e.g. Murton *et al.*, 2006) has been performed on the ice segregation process in laboratory studies. Matsuoka & Murton (2008) suggest to monitor the process in natural environments, in a context of risk assessment of rock falls and avalanches in permafrost and periglacial environments. Field monitoring of e.g. temperature and dilation on building materials have been done as well in order to understand the mechanism of frost weathering in natural environments (Thomachot *et al.*, 2005).

The prediction of the frost susceptibility of a rock in a certain climate, however, stays a delicate topic. Materials which have proven to be durable in certain regions, might respond differently and less durable when imported into other climatic regions (Cnudde *et al.*, in review). Laboratory freeze-thaw testing always seems advisable for

building materials. Nevertheless, the correlation between laboratory tests and natural environments is far from easy (Ingham, 2005). The outcome of laboratory tests should be interpreted with care. More than an absolute conclusion, the outcome is to be compared with stones whose historical performance is well known in both laboratory and natural environments. In addition, the use of indirect methods and optical petrography is an added value for the assessment of frost susceptibility. Such indirect methods are based on the pore structure or water absorption. Two parameters have been used in Belgium. Firstly, d_{10} (Ingham, 2005) is defined as the pore diameter that corresponds to a 10 cumulative-% intrusion with mercury intrusion porosimetry. Empirically, frost damage should be negligible if $d_{10} > 2.5$ µm. Secondly, the GC-coefficient (NBN B 24-213) is based on the capillary water uptake relative to the total porosity in function of time. The outcome is a number which classifies the rock for certain applications. GC values $\leq$ - 4 indicate a very good frost resistance, whereas stones with number around 0 should not be used in certain frost sensitive applications.

This work characterizes the microstructure of Massangis varieties and compares this information with the material's resistance to freeze-thaw. The Massangis stone type was selected because of its exhaustive use in Belgium and its mutual microstructural variation related to post-depositional processes within similar limestone facies. Freeze-thaw tests are performed in the laboratory to assess their behavior under freeze-thaw conditions to compare this with their microstructure and the use of indirect methods. X-ray microtomography is used for the characterization and visualization of the microstructure and damage patterns such as cracks (Jacobs *et al.*, 1997; Boone *et al.*, 2009; Ketcham *et.al.*, 2010; Dewanckele *et al.* 2011).

2. Materials and methods

2.1 Massangis

The 'extreme' Massangis varieties Massangis Roche Claire and Massangis Roche Jaune were selected as they are commercialized in Belgium. The distinction between both is obvious in its color. Alternative commercial names are Vaurion, Val d'Arion, Malpierre, Hervaux, Montaigne & Necker (Dusar *et al.*, 2009) and refer to historic excavations. The rocks are compact, oolitic and bioclastic grainstones with visible shell fragments.

2.2 Characterization methods

A Zeiss Axioscope with camera was used for petrographical description of uncovered 30 µm thin sections stained with Alizarine Red-S.

X-ray computed microtomography (µCT) was performed at the Centre for X-ray Tomography (www.ugct.ugent.be, Masschaele *et al.*, 2007). The experimental setup for the lab-based CT consisted of a FeinFocus FXE160.51 transmission tube operated at 80 kV. Projection images were recorded using a Varian 2520V Paxscan flat-panel detector. The images were processed with the in-house developed software for reconstruction (Octopus) (Dierick *et al.*, 2004; Vlassenbroeck *et al*., 2007). Image analysis was performed with the in-house developed software Morpho+ (Brabant *et al*., 2011). 3D visualisation of the CT data was done using the software package VGStudio® MAX.

Neutron radiography, an ideal technique to visualize water uptake inside rocks (Cnudde *et al.*, 2008), was performed at the NEUTRA beamline at the PSI (Villingen,

Switzerland). Due to the high difference in neutron scattering for rock and water, water uptake could be visualized in function of time.

Total open porosity and bulk density were determined according to the European standard EN 1936 (1999) using the triple weight method. A total of 50 samples, sized 50 x 50 x 50 mm³, were saturated with water under vacuum of 98.66 kPa

Total porosity and pore throat distribution was assessed using Mercury Intrustion Porosimetry (MIP). This was performed at the Magnel Laboratory for Concrete research (Ghent University, Belgium), using a Thermo Scientific Pascal 140 and Pascal 440 device. The cylindrical samples weighed in between 0.200 – 0.2500 g.

Capillary imbibition was measured on 50 cubic samples of 50 x 50 x 50 mm³ by putting them on supports in demineralized water. The change of mass due to capillary water uptake was measured in function of time. The capillary uptake parameter C [$g/m^2.\sqrt{t}$] is determined by:

$$C = x \frac{m_t - m_i}{A\sqrt{t}}$$

With m_t the weight in g at time t measured on the first slope of the curve, m_i as the initial dry weight en A as the bottom surface of the samples.

Measurements of tensile strength were performed at the Magnel Laboratory for Concrete research using a Digi Con 2000. Samples of 40 x 40 x 160 mm³ were loaded in the center until rupture. Afterwards, the resulting halves were subjected to compressive strength measurements with the same device, using a 40 x 40 mm² loading platform.

2.3 Freeze-thaw testing

Freeze-thaw testing was performed at the Magnel Laboratory for Concrete research. A total of 50 samples of 50 x 50 x 50 mm³ were saturated by progressive immersion and subsequently subjected to 25 freeze-thaw cycles according to NBN B 17-001 (1998). The first 10 cycles had a unidirectional cooling stage to -15 °C in 180 minutes, each followed by a thawing stage in a water bath at 20 °C. This was followed by 15 unidirectional cooling stages to -5 °C, again followed by a similar thawing stage.

3. Results

3.1 Massangis Roche Claire

Massangis Roche Claire is an oolitic grainstone with bioclasts such as echinoderm, shell and coral fragments (Figure 1). The fabric is grain supported with point contacts between the grains. Alizarine Red-S staining reveals a calcite composition for the ooids. A first cementation phase consists of grain-lining microsparite. Secondary, larger sparite crystals filled in the intergranular pore space and formed syntaxial overgrowth on echinoderm fragments.

A moldic mesoporosity with rhombic structure can be attributed to secondary dolomite dissolution. This can be seen on both thin sections and µCT slices (Figure 1). However, since a considerable amount of dolomite remains in the interparticular space, this dedolomitization process was limited. Interparticular mesoporosity is remnant when the accommodation is not entirely filled with cement. The ooids have microporous outer layers. This can be seen on the µCT slices, as this microporous material has a lower grey value. An intraparticular meso- to microporosity is sometimes present within the ooids, which is the result of dissolution and possible subsequent dolomite precipitation.

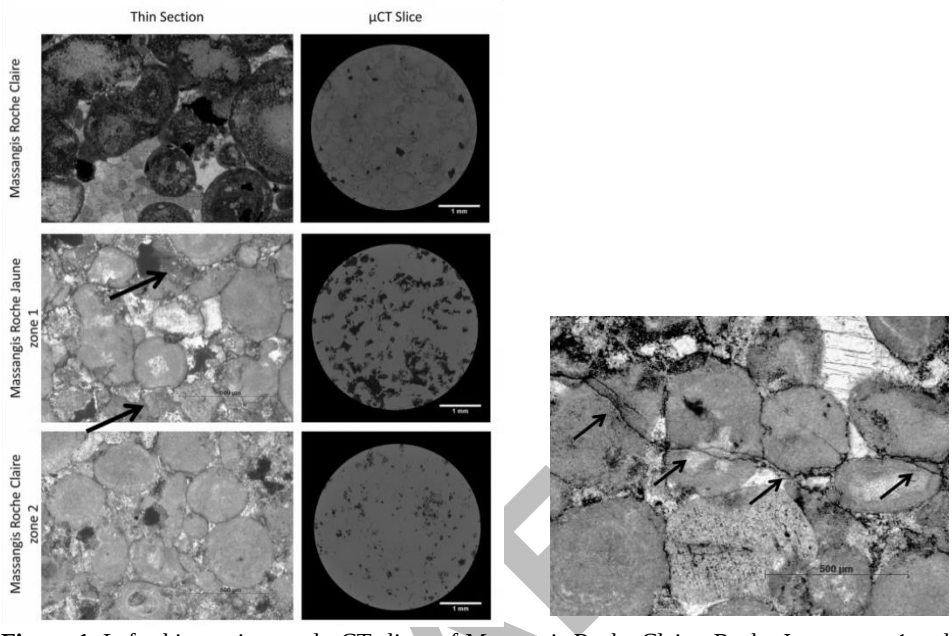

Figure 1. Left: thin sections and µCT slices of Massangis Roche Claire, Roche Jaune zone 1 and 2. Right: Cemented fissure crosscutting Massangis Roche Jaune

3.2 Massangis Roche Jaune

Massangis Roche Jaune is also a bioclastic oolitic grainstone, bus shows a different texture compared to the Roche Claire (Figure 1). The fabric is condensed grain supported with sutured contacts between the calcite ooid grain boundaries. Rhombic dolomite crystals are present at grain contacts and penetrate into the ooids without inheritance of the ooid texture. Bioclasts consist of echinoderm fragments, shell fragments and corals. The latter two have a calcite edge, but dolomitic internal structure. The cement is a combination of interfering large euhedric dolomite crystals and smaller sub- to anhedric mixed dolomite and calcite crystals. The dominant porosity is a moldic mesoporosity, resulting from the secondary dissolution of dolomite crystals. This is visible in both thin section and µCT slices (Figure 2). On µCT slices, a phase that lines the rhombic pores is discernible from the bulk mass, resulting from incomplete dolomite dissolution. Intraparticular porosity is limited to some local ooids.

However, patches with a different microstructure in the magnitude of several cm^3, occur randomly within the bulk of the Roche Jaune (Figure 1). The latter is referred to as zone 1, while the patches are referred to as zone 2. Zone 2 has similar allochems with sutured contacts, but a lower porosity compared to zone 1. Striking is the absence of euhedric dolomite crystals in comparison to zone 1. Rhombic interparticular porosity suggests the preferential secondary dissolution of dolomite crystals in zone 2, but their size and abundance is rather small in comparison to zone 1. The interparticular cementation in zone 2 consists a first microsparite cement lining the allochems where no

contact dissolution occurred and a second pore filling microsparite mixed dolomite and calcite cement.

Dolomite cemented fissures pierce the fabric and crosscut grains, sutured grain boundaries and microsparite cement (Figure 1). Euhedric dolomite crystals or rhombic moldic porosity occur along this cemented fissures and therefore seem to be related.

3.3 Microstructure

Several techniques were used to characterize the microstructure of Roche Claire and Roche Jaune (Table 1). When possible, the bulk (zone 1) and the patches (zone 2) were treated separately. The different microstructure observed in thin section and µCT slices is reflected by the results of water absorption and mercury intrusion porosimetry (Table 1 and 2). A significant difference exists in absolute results between the Roche Claire and Roche Jaune, but also within the Roche Jaune a high variability becomes clear.

In general, the Roche Claire has the highest total porosity determined by both water absorption and MIP. From a total porosity of 13.81 vol-%, 87 % is filled with water under atmospheric pressure. MIP reveals a high microporosity for the Roche Claire: over 95 % of the pores have a pore throat smaller than 1 µm.

In contrast, the general total porosity of the Roche Jaune is lower (10.65 vol-%). Only 70 % of the pore volume fills under atmospheric pressure conditions. The proportion of macro- and mesopores is higher in comparison to the Roche Claire. However, zone 1 and zone 2, show a distinct mutual variance, which makes it ambiguous to generalize the Roche Jaune results. Results from MIP show that the total porosity of zone 1 (13.02 vol-%) is similar to or even exceeds the total porosity of Roche Claire (11.82 vol-%), whereas the total porosity of zone 2 (2.11 vol-%) is much lower. Both have a lower vol-% of microporosity compared to the Roche Claire. The amount of meso-and macroporosity which is present is zone 1, however, lacks in zone 2 which is reflected in the critical and mean pore diameter as determined by MIP.

The tensile strength of both rocks is in the same order of magnitude (Table 1) . The compressive strength of the Roche Jaune is higher than the Roche Claire. However, there is a high uncertainty on the results. The measured difference between samples which were separated by only 5 cm in the bedding was up to 67.12 N/mm². This once again reflects the large heterogeneity in the Roche Jaune.

	Porosity [vol-%]	Saturation coefficient	Capillary Uptake Parameter [g/(m²√t)]	GC-coefficient	Tensile Strength [Nmm²]	Compressive Strength [N/mm²]
Massangis Roche Claire	13.81 ± 0.34	0.87 ± 0.02	58.00 ± 4.70	2.06 ± 0.58	4.03	67.69 ± 7.78
Massangis Roche Jaune	10.65 ± 2.48	0.70 ± 0.10	51.41 ± 33.20	-5.37 ± 4.28	4.30	90.43 ± 28.67

Table 1. Results of petrophysical testing

	Total porosity (vol-%)	Critical diameter [µm]	Median diameter [µm]	*d10* [µm]
Massangis Roche Claire	11.82	0.32 – 0.23	0.22	0.32
Massangis Roche Jaune zone 1	13.07	2.14 – 1.62	3.02	19.98
Massangis Roche Jaune zone 2	2.11	0.23	0.09	3.43

Table 2. Results of MIP

3.4 Indirect methods

Both Roche Claire and Roche Jaune have different capillary uptake parameters. Whilst the capillary uptake is homogeneous Roche Clair, a huge variability exists within the Roche Jaune. This is visualized by time-lapse neutron images of the capillary uptake (Figure 2). Instead of a steady moving capillary front, the uptake has preferential pathways and results in locations of higher saturation. These 'clouds' of capillary uptake follow preferentially zone 1. Moreover, zone 2 seems to have no capillary uptake at all. When samples are left in place for several weeks, zone 2 areas remain dry whereas neighboring zone 1 areas are saturated. Zone 2 has thus a closed porosity or is separated from zone 1 by a clogged border.

The GC-coefficient is derived from this capillary uptake thus different GC-coefficients can be expected not only for Roche Claire and Roche Jaune, but also for Roche Jaune zone 1 and 2 (Table 1). However, because of the irregular distribution, zone 1 and 2 could not be measured separately. Instead, the high standard deviation is the result of different relative proportions of zone 1 versus zone 2. Despite of the average result (-5.37) which states the Roche Jaune has a very good frost resistance in general, there is a larger spread on a more detailed scale.

µCT was used to assess the mesoporosity. Pores with an equivalent diameter ≥ 7.47 µm (3 voxels) were analyzed with Morpho+. In essence, this is the moldic and interparticular mesoporosity. For each separate pore, the equivalent diameter was calculated together with the amount of neighboring pores it is connected to. The amount of connected neighbors for a given porosity is a fivefold for the Roche Jaune compared to Roche Claire.

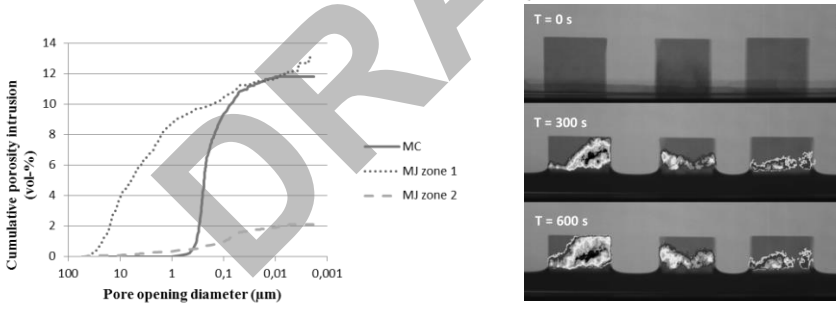

Figure 2. Left: Cumulative pore opening diameter with MIP. Right: time-lapse visualization of capillary water uptake with neutron radiography. Grey values reflect the amount of water inside the stone and the heterogeneity of the water-uptake is visible

3.5 Direct testing

After 25 freeze-thaw cycles, the hand sized specimen were subjected to visual inspection (Figure 3) and determination of weight loss. In term of weight loss, the damage was low with an average of approximately -0.15 mass-% with a maximum of -1.19 mass-% for the Roche Claire and less than 0.01 mass-% for the Roche Jaune.

The observed damage was different for both varieties. Chipping was the common damage on the Roche Claire at the edges exposed to unidirectional cooling. 1 out of 3 blocks showed significant chipping. Minor chipping occurred at 1 out of 10 samples Roche Jaune. However, fissures and fractures are the more important damage patterns. 1

out of 6 samples shows fissures or fractures. These fissures all occur in zone 1. On µCT images of a fracture (Figure 3), it can be seen that this fracture is lined with the same phase that is remnant in the rhombic structures. It can be suggested this pore-filling phase is a preferential direction for fissuring, when it forms a continuous body.

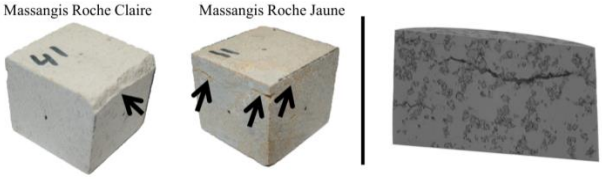

Figure 3. Representative examples of observed damage. Left: chipping (arrows) at the edges of Roche Claire and fracture (arrows) in Roche Jaune. Right: 3D rendering of fracture in Roche Jaune

4. Discussion

There is a large difference in microstructure between Roche Claire and Roche Jaune. This is the result of different post-depositional processes such as compaction, pressure solution and dolomitization/dedolomitization. Limited compaction caused a grain supported fabric in the Roche Claire with an interparticular accommodation space which was cemented and closed by dolomite cement phases. Limited dedolomitization gave rise to a low percentage of moldic mesoporosity. However, intraparticular porosity in the ooids make up most of the pore space. The Roche Jaune has a more condensed fabric with sutured grain contacts. Intense dolomitization occurred in the bulk of the Roche Jaune (zone 1), however, patches with a lower degree of dolomitization (zone 2) occur randomly throughout the bulk. Both zone 1 and zone 2 have a microporosity of approximately 2 vol-%. In contrast to the Roche Claire, this cannot be observed inside the ooids and this porosity could thus be related to the dolomitization process. Later dedolomitization was more pronounced in zone 1 because of the higher abundancy of dolomite. This created a moldic mesoporosity which is unique for the Roche Jaune.

The GC-coefficient and d_{10} point out a possible frost susceptibility for the Roche Claire. This is the expression of the high microporosity remnant in the ooids. Based on d_{10}, the Roche Claire (0.32 µm) could be sensitive to frost action. In contrast, these parameters suggest a good frost resistance for the Roche Jaune. This is the expression of differences in microstructure between both varieties. Whilst the Roche Claire has the highest average porosity, it also has the highest percentage of micropores and in contrast to Roche Jaune, mesopores which can act as accommodation space for ice growth or expelled water are 5 times more isolated according to the µCT analysis. The difference between zone 1 and zone 2 is again reflected in d_{10}. Roche Jaune zone 1 should not be frost sensitive with a $d_{10\,of}$ 19.98 µm. Zone 2 is also not suggested to be frost sensitive, but its d_{10} (3.43 µm) is positioned much closer to the empirical boundary parameter of 2.5 µm.

Based on thin sections, µCT and capillary water uptake, two zones could be recognized in the Roche Jaune which are responsible for the high heterogeneity within the rock and therefore should be treated separately. However, while zone 2 can be indicated as potentially susceptible to frost by indirect methods, this zone has not the

intention of absorbing water, even when the surrounding is saturated. Potential damage however, could occur at the edge between zone 1 and zone 2, where pore waters from a saturated zone 1 are retained from migration.

Freeze-thaw testing illustrate that the Roche Claire and Roche Jaune have a different frost susceptibility, with chipping damage for Roche Claire and fissures and fractures developing in the Roche Jaune. The difference in deterioration is not related to technical properties such as the tensile strength as these are similar. Both had the same freeze-thaw regime. This suggests the difference in damage arises from their different microstructure.

5. Conclusions

The observations of freeze-thaw testing suggest that the microstructure of Roche Claire is most prone to consequent freeze-thaw deterioration by chipping at the surface. However, the most severe damage occurs in the Roche Jaune. Fissures and fractures seem to be associated with the dolomite phase on places with a higher connectivity. Cemented fissures as observed in thin section might be such a place.

Indirect methods such as the GC-coefficient and d_{10} are reliable methods for the assessment of frost susceptibility (see also: Ingham, 2005) in homogeneous rocks such as Roche Claire. Intuitive interpretations of the relationship between microstructure and frost susceptibility are reflected by these quantitative parameters. However, unconformities in the rock fabric may induce damage, as observed in the Roche Jaune.

Although the varieties between Roche Claire and Roche Jaune, as mentioned in the introduction, are not presented in this work, the Massangis Roche Jaune Claire was incorporated in earlier freeze-thaw testing (De Kock, 2009). These blocks showed little damage. Future work might find out if they lack the zones which cause fracturing.

Acknowledgements

The authors would like to thank the Agency for Promotion of Innovation by Science and Technology in Flanders, Belgium (IWT) for the PhD grant of J. Dewanckele.

References

Boone, M.A., De Kock, T., Dewanckele, J. *et al.* 2009. 'Three-dimensional monitoring of physical weathering in limestone with X-ray computed microtomography (micro-CT)'. Paper presented at the 12th Euroseminar on Microscopy Applied to Building Materials, Dortmund, 15-19 September 2009.

Brabant, L., J. Vlassenbroeck, *et al.* 2011. 'Three-Dimensional Analysis of High-Resolution X-Ray Computed Tomography Data with Morpho+.' *Microscopy and Microanalysis* **17**(2): 252-263.

Breda, K., 2005. 'De 'carrière' van een architect'. Paper presented at Eerste Vlaams-Nederlandse natuursteendag, , Leuven, 3 February, 2005.

Camerman, C, 1957. *Beschrijving en gebruik in België en Nederland van de Franse witte steen.* Hayez, Brussel, 100p.

Casteleyn, L., P. Robion, *et al.* 2010. 'Interrelations of the petrophysical, sedimentological and microstructural properties of the Oolithe Blanche Formation (Bathonian, saline aquifer of the Paris Basin).' *Sedimentary Geology* **230**(3-4): 123-138.

Cnudde, V.; Dierick, M.; Vlassenbroeck, J. *et al*. 2008.' High-speed neutron radiography for monitoring the water absorption by capillarity in porous materials'. *Nuclear instruments & methods in physics research section b-beam interactions with materials and atoms.* ***266****(1:)* 155-163.

Cnudde, V., De Boever, W., Dewanckele, J. *et al.*, in review. Multi-disciplinary characterisation and monitoring of sandstone (Kandla Grey) under different external conditions. Quarterly Journal of Engineering Geology and Hydrogeology.

De Kock, T. 2009. De Ledesteen en zijn hedendaagse vervangstenen. Master dissertation. Department of Geology and Soil Science, Ghent University.

Dessandier, D., avec la collaboration de G. Ambroise & A. Longet 2006 . Mémento des pierres ornementales et de construction de la région Bourgogne. BRGM/RP-54614-FR, 294 p., 7 fig., 6 tab., 2 ann.

Dewanckele, J., T. De Kock, *et al.*, 2011. '4D imaging and quantification of pore structure modifications inside natural building stones by means of high resolution X-ray CT.' *Science of the Total Environment* **416**: 436-448.

Dierick, M., Masschaele, B., Van Hoorebeke, L. (2004). 'Octopus, a fast user-friendly tomographic reconstruction package developed in LabView®'. *Measurement Science and Technology*, **15**, 1366-1370.

Dusar, M., Dreesen, R., De Naeyer, A., 2009. *Renovatie & restauratie. Natuursteen in Vlaanderen, versteend verleden*. Kluwer, Mechelen, 562 p.

Elsen, J., Van Kriekingen, H. & Swennen, R., 2007. Polarisation fluorescence microscopy as a tool to assess the frost resistance of building stone – the French Massangis building stone as a case-study. Paper presented at the 11th Euroseminar on Microscopy Applied to Building Materials, Porto, 5-9 June 2007.

Ketcham, R. A., D. T. Slottke, *et al.* 2010. 'Three-dimensional measurement of fractures in heterogeneous materials using high-resolution X-ray computed tomography.' *Geosphere* **6**(5): 499-514.

Masschaele, B.C., Cnudde, V., Dierick, M., *et al.* 2007. 'UGCT: New X-ray Radiography and Tomography Facility', *NIM A*, **580**, 266-269.

Matsuoka, N. and Murton, J. 2008. 'Frost weathering: Recent advances and future directions.' *Permafrost and Periglacial Processes* **19**(2): 195-210.

Murton, J. B., R. Peterson, *et al.* 2006. 'Bedrock fracture by ice segregation in cold regions.' *Science* **314**(5802): 1127-1129.

Ingham, J. P. 2005. 'Predicting the frost resistance of building stone.' *Quarterly Journal of Engineering Geology and Hydrogeology* **38**: 387-399.

Jacobs, P., E. Sevens, *et al.* 1997. 'Non-destructive monitoring of interactive physical and biological deterioration of building stones by computerized X-ray tomography.' Rotterdam, A a Balkema.

Ruedrich, J., Siegesmund; S. 2007. 'Salt and ice crystallisation in porous sandstones.' *Environmental Geology* **52**(2): 343-367.

Tharp, T. M. (1987). 'Conditions for crack-propagation by frost wedging.' *Geological Society of America Bulletin* **99**(1): 94-102.

Thomachot, C., Matsuoka, N. *et al*. 2005. 'Frost damage of bricks composing a railway tunnel monument in Central Japan: field monitoring and laboratory simulation.' *Natural Hazards and Earth System Sciences* **5**(4): 465-476.

Vlassenbroeck, J., Dierick, M., Masschaele, B., *et al*. 2007. 'Software tools for quantification of X-ray microtomography at the UGCT, Nuclear Instruments and Methods.' *Physics Research Section A: Accelerators, Spectrometers, Detectors and Associated Equipment*, Volume **580**, pp. 442–445.

Walder, J. and Hallet, B. 1985. 'A theoretical-model of the fracture of rock during freezing.' *Geological Society of America Bulletin* **96**(3): 336-346.

Walder, J. S. and Hallet, B. 1986. 'The physical basis of frost weathering - toward a more fundamental and unified perspective.' *Arctic and Alpine Research* **18**(1): 27-32.